

STATIC BENDING AND FREE VIBRATION ANALYSIS OF FUNCTIONALLY GRADED POROUS PLATES LAID ON ELASTIC FOUNDATION USING THE MESHLESS METHOD

Vu Tan Van^{a,*}, Nguyen Huynh Tan Tai^b, Nguyen Ngoc Hung^c

^a*Department of Civil Engineering, University of Architecture Ho Chi Minh City, 196 Pasteur street, District 3, Ho Chi Minh city, Vietnam*

^b*Faculty of Civil Engineering, Ho Chi Minh City University of Technology and Education, 1 Vo Van Ngan street, Thu Duc district, Ho Chi Minh city, Vietnam*

^c*Faculty of Architecture, Thu Dau Mot University, 6 Tran Van On street, Thu Dau Mot city, Binh Duong province, Vietnam*

Article history:

Received 25/12/2020, Revised 22/02/2021, Accepted 26/02/2021

Abstract

This paper presents a numerical approach for static bending and free vibration analysis of the functionally graded porous plates (FGPP) resting on the elastic foundation using the refined quasi-3D sinusoidal shear deformation theory (RQSSDT) combined with the Moving Kriging–interpolation meshfree method. The plate theory considers both shear deformation and thickness-stretching effects by the sinusoidal distribution of the in-plane displacements, satisfies the stress-free boundary conditions on the top and bottom surfaces of the plate without shear correction coefficient. The advantage of the plate theory is that the displacement field of plate is approximated by only four variables leading to reduce computational efforts. Comparison studies are performed for the square FGPP with simply supported all edges to verify the accuracy of the present approach. The effect of the aspect ratio, volume fraction exponent, and elastic foundation parameters on the static deflections and natural frequency of FGPP are also investigated and discussed.

Keywords: meshless method; Moving Kriging interpolation; refined quasi-3D theory; porous functionally graded plate; Pasternak foundation.

[https://doi.org/10.31814/stce.nuce2021-15\(2\)-12](https://doi.org/10.31814/stce.nuce2021-15(2)-12) © 2021 National University of Civil Engineering

1. Introduction

It is well known that the functionally graded materials (FGM) are the two-component composite characterized by a compositional gradient from one component to the other. Therefore, they involve a compromise between the desirable properties of the component materials. As a result, one can employ them in many structures worked in the harsh environment. However, in the process of FGM manufacturing, porosities can generate inside the materials during the sintering action because of the enormous difference in solidification temperatures between material components [1].

*Corresponding author. *E-mail address:* van.vutan@uah.edu.vn (Van, V. T.)

Up to now, the interaction between FGM structures and supported elastic media has been considered by many researchers (e.g. [2]). It should be recalled that the simple foundation model was first discussed by Winkler [3] for the one-parameter elastic foundation, and then Pasternak [4] suggested a two-parameter foundation model for analyzing the elastic foundations. Recently, Kerr [5] presented a three-parameter foundation model for the elastic and viscoelastic foundations.

In order to analyze the problem of functionally graded porous plates (FGPP) laid on elastic foundations, one can utilize the two-dimensional shear deformation theories such as the classical plate theory proposed by Kirchhoff [6], the first-order shear deformation theory developed by Mindlin [7], or Reissner [8], and the higher-order shear deformation theories (e.g. [9]), and the refined plate theory [10].

It is worth noting that these two-dimensional shear deformation theories neglect the effect of thickness stretching (i.e. $\varepsilon_{zz} = 0$) since the transverse displacement is assumed constant across the plate thickness. However, this thickness stretching effect should be taken into consideration for thick plate analysis, according to Carrera *et al.* [11]. To overcome the drawback of the previous two-dimensional shear deformation theories, a class of quasi-3D shear deformation theories, based on the quadratic variations along with the plate thickness for the transverse displacement, were proposed for taking the thickness stretching effect. Many of them are computationally cumbersome since they included a vast amount of unknown variables (e.g. [12–18]), only a few of the quasi-3D shear deformation theories have five [19, 20] or four unknown variables [21].

Nevertheless, one of the main conveniences of the simple quasi-3D shear deformation theory [21] is that it requires the shape functions for the displacement fields should be at least C^1 continuous, thus hindering the natural use of the traditional finite element method. One of the best ways to overcome this obstacle is to utilize the meshfree or meshless methods (MMs) with shape functions that could be constructed for any the desired order continuity. To the best of the authors' knowledge, there is no numerical approach on the static bending and free vibration analysis of the FGM plate with porosity resting on the elastic foundation based on the moving Kriging interpolation-based element-free Galerkin method and refined quasi-3D shear deformation theory.

In this paper, using the refined quasi-3D sinusoidal shear deformation theory wherein the effect of transverse shear and normal strain are considered and combined with the enhanced moving Kriging interpolation-based (EMKI) element-free Galerkin method [22], the static bending and free vibration analysis of simply supported functionally graded porous rectangular plates resting on two-parameter elastic foundation is numerically investigated.

We organize the rest of the paper as follows. Section 2 presents the theoretical models for FGPP plates and the mathematical modeling of the RQSSDT with its displacement field, constitutive relations, and the total potential energy. Section 3 outlines the EMKI based-meshless method, the discrete formulations for analysis of the static bending and free vibration of the FGPP rested on the elastic foundations. Section 4 presents several numerical validations and parametric studies. Finally, several conclusions drawn from the present study are outlined in Section 5.

2. Theoretical formulation

2.1. Description of the FGPP

Consider an FGM plate has a uniform thickness h , length a , and width b laid on the elastic foundation characterized by parameters of k_w and k_s are shown in Fig. 1(a). The Cartesian coordinates system with an origin $(0, 0, 0)$ located at the center of the middle surface of the plate. Assuming

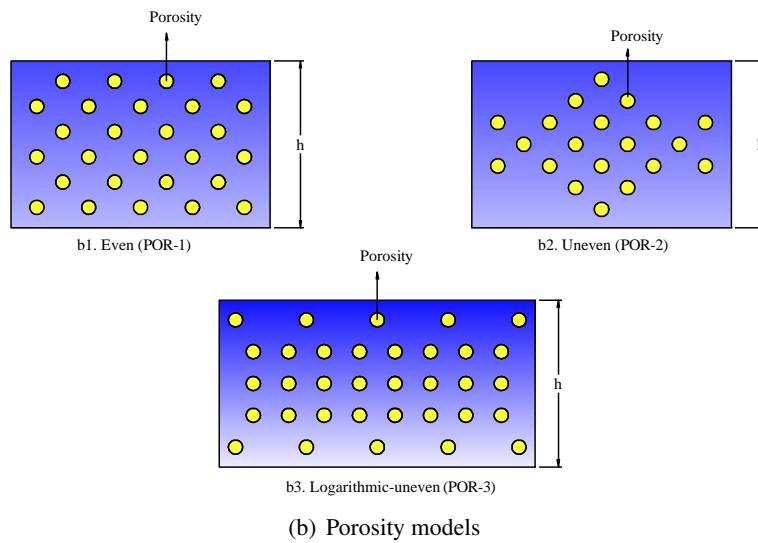
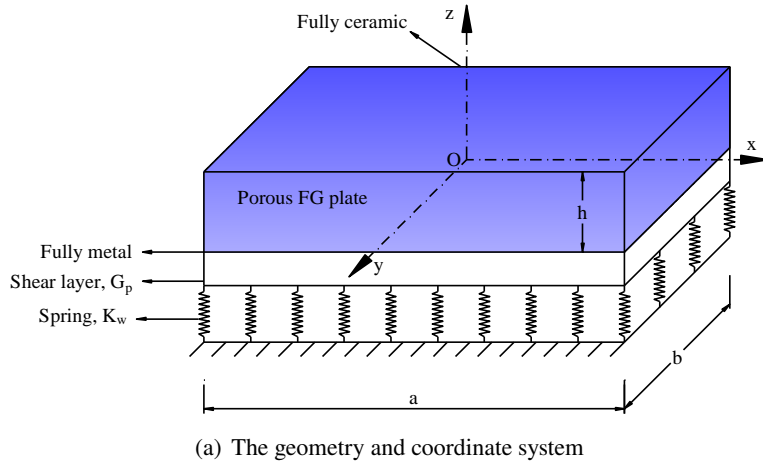


Figure 1. The configuration of rectangular FGPP laid on two-parameter foundation

that the effective properties comprised Young modulus $E_{eff}(z)$ and mass density $\rho_{eff}(z)$ that varied through the plate thickness by the power-law distribution in Voigt's model, while the Poisson's ratio ν is constant. Three types of porosity distributions across the plate thickness as follow:

a. FGPP with even porosities (POR-1)

The distribution of porosities inside the plate may exist during the production, the effective material properties of the FGPP with even porosities (as shown in Fig. 1(b).1) can be described by the modified mixture rule as follow [23]

$$E_{eff}(z) = (E_c - E_m) \left(\frac{z}{h} + \frac{1}{2} \right)^\chi + E_m - \frac{\vartheta}{2} (E_c + E_m) \quad (1)$$

$$\rho_{eff}(z) = (\rho_c - \rho_m) \left(\frac{z}{h} + \frac{1}{2} \right)^\chi + \rho_m - \frac{\vartheta}{2} (\rho_c + \rho_m) \quad (2)$$

where subscripts of c and m denote the ceramic and metal, respectively. Also, χ represents the power-law exponent or gradient index defined the material variation across the plate thickness, and ϑ ($0 \leq \vartheta < 1$) is the porosity volume fraction.

b. FGPP with uneven porosities (POR-2)

The second model for the distribution of porosities inside the plate based on the uneven rule, the effective material properties of this FGPP with uneven porosities (as shown in Fig. 1(b).2) as follow [23]

$$E_{eff}(z) = (E_c - E_m) \left(\frac{z}{h} + \frac{1}{2} \right)^\chi + E_m - \frac{\vartheta}{2} (E_c + E_m) \left(1 - \frac{2|z|}{h} \right) \quad (3)$$

$$\rho_{eff}(z) = (\rho_c - \rho_m) \left(\frac{z}{h} + \frac{1}{2} \right)^\chi + \rho_m - \frac{\vartheta}{2} (\rho_c + \rho_m) \left(1 - \frac{2|z|}{h} \right) \quad (4)$$

c. FGPP with logarithmic-uneven porosities (POR-3)

The third model for the distribution of porosities inside the plate based on the logarithmic-uneven rule, the effective material properties of this FGPP with uneven porosities (as shown in Fig. 1(b).3) as follow [19]

$$E_{eff}(z) = (E_c - E_m) \left(\frac{z}{h} + \frac{1}{2} \right)^\chi + E_m - \log \left(1 + \frac{\vartheta}{2} \right) (E_c + E_m) \left(1 - \frac{2|z|}{h} \right) \quad (5)$$

$$\rho_{eff}(z) = (\rho_c - \rho_m) \left(\frac{z}{h} + \frac{1}{2} \right)^\chi + \rho_m - \log \left(1 + \frac{\vartheta}{2} \right) (\rho_c + \rho_m) \left(1 - \frac{2|z|}{h} \right) \quad (6)$$

2.2. Refined quasi-3D sinusoidal shear deformation theory

Assuming that \mathfrak{J} is a domain cover by the middle surface of the plate, the displacement field $u(x, y, z, t)$, $v(x, y, z, t)$ and $w(x, y, z, t)$ accounted for the effect of transverse shear and normal deformation [18], is expressed:

$$u(x, y, z, t) = u_0(x, y, t) - z \frac{\partial w_b(x, y, t)}{\partial x} + f(z) \frac{\partial w_s(x, y, t)}{\partial x} \quad (7)$$

$$v(x, y, z, t) = v_0(x, y, t) - z \frac{\partial w_b(x, y, t)}{\partial y} + f(z) \frac{\partial w_s(x, y, t)}{\partial y} \quad (8)$$

$$w(x, y, z, t) = w_b(x, y, t) + w_s(x, y, t)g(z) \quad (9)$$

where t represents the time; $u_0(x, y, t)$, $v_0(x, y, t)$ and $w_b(x, y, t)$ are the displacements of the middle plane ($z = 0$) with respect to the x, y and z direction, respectively; and $w_s(x, y, t)$ is an additional displacement that considered an effect of normal stress. The proposed transverse shear deformation functions, chosen carefully so that satisfying naturally the vanished condition at the outer surfaces of plate for transverse shear stresses, are $f(z) = \sin(\pi z/h)$ [24] and $g(z) = \pi \cos(\pi z/h)/3h$, respectively. On the other hand, Eqs. (7)–(9) can be expressed in the matrix form:

$$\bar{\mathbf{w}} = \bar{\mathbf{w}}_1 + z\bar{\mathbf{w}}_2 + f(z)\bar{\mathbf{w}}_3 + g(z)\bar{\mathbf{w}}_4 \quad (10)$$

where

$$\bar{\mathbf{w}}_1 = \left\{ \begin{array}{c} u_0 \\ v_0 \\ w_b \end{array} \right\} \quad (11)$$

$$\bar{\mathbf{w}}_2 = - \begin{pmatrix} \partial w_b / \partial x \\ \partial w_b / \partial y \\ 0 \end{pmatrix} \quad (12)$$

$$\bar{\mathbf{w}}_3 = \begin{pmatrix} \partial w_s / \partial x \\ \partial w_s / \partial y \\ 0 \end{pmatrix} \quad (13)$$

$$\bar{\mathbf{w}}_4 = \begin{pmatrix} 0 \\ 0 \\ w_s \end{pmatrix} \quad (14)$$

Assuming that the plate material is linearly elastic, and strains are small, the strain–displacement relations can be stated as follows:

$$\bar{\boldsymbol{\varepsilon}} = \left\{ \varepsilon_{xx} \quad \varepsilon_{yy} \quad \gamma_{xy} \quad \varepsilon_{zz} \right\}^T = \bar{\boldsymbol{\varepsilon}}_1 + z\bar{\boldsymbol{\varepsilon}}_2 + f(z)\bar{\boldsymbol{\varepsilon}}_3 + g'(z)\bar{\boldsymbol{\varepsilon}}_4 \quad (15)$$

$$\boldsymbol{\gamma} = \left\{ \gamma_{xz} \quad \gamma_{yz} \right\}^T = [f'(z) + g(z)] \bar{\boldsymbol{\varepsilon}}_s \quad (16)$$

where

$$\bar{\boldsymbol{\varepsilon}}_1 = \begin{pmatrix} \frac{\partial u_0}{\partial x} \\ \frac{\partial v_0}{\partial y} \\ \frac{\partial u_0}{\partial y} + \frac{\partial v_0}{\partial x} \\ 0 \end{pmatrix} \quad (17)$$

$$\bar{\boldsymbol{\varepsilon}}_2 = - \begin{pmatrix} \frac{\partial^2 w_b}{\partial x^2} \\ \frac{\partial^2 w_b}{\partial y^2} \\ 2 \frac{\partial^2 w_b}{\partial x \partial y} \\ 0 \end{pmatrix} \quad (18)$$

$$\bar{\boldsymbol{\varepsilon}}_3 = \begin{pmatrix} \frac{\partial^2 w_s}{\partial x^2} \\ \frac{\partial^2 w_s}{\partial y^2} \\ 2 \frac{\partial^2 w_s}{\partial x \partial y} \\ 0 \end{pmatrix} \quad (19)$$

$$\bar{\boldsymbol{\varepsilon}}_4 = \begin{pmatrix} 0 \\ 0 \\ 0 \\ w_s \end{pmatrix} \quad (20)$$

$$\bar{\varepsilon}_s = \left\{ \begin{array}{c} \frac{\partial w_s}{\partial x} \\ \frac{\partial w_s}{\partial y} \end{array} \right\} \quad (21)$$

where $f'(z) = \frac{df(z)}{dz}$, and $g'(z) = \frac{dg(z)}{dz}$. The stress-strain relationships can be expressed in the general Hooke's law as follows:

$$\left\{ \begin{array}{c} \sigma_{xx} \\ \sigma_{yy} \\ \sigma_{zz} \\ \tau_{yz} \\ \tau_{xz} \\ \tau_{xy} \end{array} \right\} = \left\{ \begin{array}{cccccc} Q_{11}(z) & Q_{12}(z) & Q_{13}(z) & 0 & 0 & 0 \\ Q_{12}(z) & Q_{22}(z) & Q_{23}(z) & 0 & 0 & 0 \\ Q_{13}(z) & Q_{23}(z) & Q_{33}(z) & 0 & 0 & 0 \\ 0 & 0 & 0 & Q_{44}(z) & 0 & 0 \\ 0 & 0 & 0 & 0 & Q_{55}(z) & 0 \\ 0 & 0 & 0 & 0 & 0 & Q_{66}(z) \end{array} \right\} \left\{ \begin{array}{c} \varepsilon_{xx} \\ \varepsilon_{yy} \\ \varepsilon_{zz} \\ \varepsilon_{yz} \\ \varepsilon_{xz} \\ \varepsilon_{xy} \end{array} \right\} \quad (22)$$

where $\sigma = \{\sigma_{xx} \ \sigma_{yy} \ \sigma_{zz} \ \tau_{yz} \ \tau_{xz} \ \tau_{xy}\}^T$ and $\varepsilon = \{\varepsilon_{xx} \ \varepsilon_{yy} \ \varepsilon_{zz} \ \varepsilon_{yz} \ \varepsilon_{xz} \ \varepsilon_{xy}\}^T$ are stress tensor and strain tensor, respectively. The elastic coefficients $Q_{ij}(z)$ can be given below:

$$Q_{11}(z) = Q_{22}(z) = Q_{33}(z) = \frac{E_{eff}(z)(1-\nu)}{(1-2\nu)(1+\nu)} \quad (23)$$

$$Q_{12}(z) = Q_{13}(z) = Q_{23}(z) = \frac{E_{eff}(z)\nu}{(1-2\nu)(1+\nu)} \quad (24)$$

$$Q_{44}(z) = Q_{55}(z) = Q_{66}(z) = \frac{E_{eff}(z)}{2(1+\nu)} \quad (25)$$

It should be noted that the effective modulus $E_{eff}(z)$ and elastic coefficients $Q_{ij}(z)$ ($i, j = 1, \dots, 6$) are changed through the plate thickness since they reference to Eq. (1). Considering an FGPP laid on the two-parameter foundation, the total potential energy Ξ can be stated [25] as follows:

$$\begin{aligned} \Xi = & \frac{1}{2} \int_V [\sigma_{xx}\varepsilon_{xx} + \sigma_{yy}\varepsilon_{yy} + \sigma_{zz}\varepsilon_{zz} + \tau_{xz}\gamma_{xz} + \tau_{yz}\gamma_{yz} + \tau_{xy}\gamma_{xy} - \rho(z)(\dot{u}^2 + \dot{v}^2 + \dot{w}^2)] dV + \dots \\ & + \frac{1}{2} \int_{\Theta} \left\{ k_w w^2 + k_s \left[\left(\frac{\partial w}{\partial x} \right)^2 + \left(\frac{\partial w}{\partial y} \right)^2 \right] + q_0 w \right\} d\Theta \end{aligned} \quad (26)$$

where q_0 denotes the transverse loading per unit; k_w and k_s are the spring and shear stiffness coefficients of the elastic foundation, respectively.

3. MKI-based meshfree method for analyzing the FGPP rested on the elastic foundations

3.1. The moving Kriging interpolation (MKI)

Consider the distribution function $u(\mathbf{x}_i)$ defined in the sub-domain φ_x ($\varphi_x \subseteq \Theta$) using n scattered nodes $\mathbf{x}_1, \mathbf{x}_2, \dots, \mathbf{x}_n$. According to framework of MKI-based meshless method [26], the MK interpolation function $\tilde{u}^h(\mathbf{x})$, $\forall \mathbf{x} \in \varphi_x$ can be approximated as follows:

$$\tilde{u}^h(\mathbf{x}) = [\mathbf{p}^T(\mathbf{x})\mathbf{A} + \mathbf{r}^T(\mathbf{x})\mathbf{B}] \mathbf{u}(\mathbf{x}) \quad (27)$$

or

$$\tilde{u}^h(\mathbf{x}) = \sum_{I=1}^n Z_I(\mathbf{x})\mathbf{u}_I \quad (28)$$

in which the MK shape function $Z_I(\mathbf{x})$ is expressed by:

$$Z_I(\mathbf{x}) = \sum_{j=1}^m p_j(\mathbf{x})A_{jI} + \sum_{k=1}^n r_k(\mathbf{x})B_{kI} \quad (29)$$

the matrices \mathbf{A} and \mathbf{B} are defined by

$$\mathbf{A} = (\mathbf{P}^T \mathbf{R}^{-1} \mathbf{P})^{-1} \mathbf{P}^T \mathbf{R}^{-1} \quad (30)$$

$$\mathbf{B} = \mathbf{R}^{-1} (\mathbf{I} - \mathbf{P}\mathbf{A}) \quad (31)$$

where \mathbf{I} is an identity matrix, $\mathbf{p}^T(\mathbf{x})$ in Eq. (27) denotes the vector with m polynomial basis functions as follows:

$$\mathbf{p}^T(\mathbf{x}) = [p_1(\mathbf{x}), p_2(\mathbf{x}), \dots, p_m(\mathbf{x})] \quad (32)$$

Also, $\mathbf{P}_{n \times m}$ in Eq. (30) comprised the values of the essential functions defined by Eq. (32) at the given nodes, is calculated by:

$$\mathbf{P}_{n \times m} = \begin{bmatrix} p_1(\mathbf{x}_1) & p_2(\mathbf{x}_1) & \cdots & p_m(\mathbf{x}_1) \\ p_1(\mathbf{x}_2) & p_2(\mathbf{x}_2) & \cdots & p_m(\mathbf{x}_2) \\ \vdots & \vdots & \ddots & \vdots \\ p_1(\mathbf{x}_n) & p_2(\mathbf{x}_n) & \cdots & p_m(\mathbf{x}_n) \end{bmatrix} \quad (33)$$

the vector $\mathbf{r}^T(\mathbf{x})$ in Eq. (27) is expressed by:

$$\mathbf{r}^T(\mathbf{x}) = [R(\mathbf{x}_1, \mathbf{x}), R(\mathbf{x}_2, \mathbf{x}), \dots, R(\mathbf{x}_n, \mathbf{x})] \quad (34)$$

in which $R(\mathbf{x}_i, \mathbf{x}_j)$ is the correlation function for arbitrary nodes \mathbf{x}_i and \mathbf{x}_j , it characteristics of the covariance $R(\mathbf{x}_i, \mathbf{x}_j) = \text{cov}[u(\mathbf{x}_i), u(\mathbf{x}_j)]$ and $R(\mathbf{x}_i, \mathbf{x}) = \text{cov}[\mathbf{u}(\mathbf{x}_i), \mathbf{u}(\mathbf{x})]$ with respect to the value field of $\mathbf{u}(\mathbf{x})$. Since using the traditional Gaussian function for the correlation function with a correlation parameter may lead to the instability numerical solutions, hence we use the multi-quadric function for the correlation function without using any correlation parameters [22] defined by:

$$R(\mathbf{x}_i, \mathbf{x}_j) = \sqrt{\left(\frac{1}{2l_x^2}\right)^2 + r_{ij}^2} \quad (35)$$

where l_x denotes the mean distance between the nodes $\mathbf{x}_i (i = 1, \dots, n)$ inside a support domain; Euclidean distance $r_{ij} = \|\mathbf{x}_i - \mathbf{x}_j\|$. The so-called correlation matrix $\mathbf{R}[R(\mathbf{x}_i, \mathbf{x}_j)]_{n \times n}$ is calculated by:

$$\mathbf{R}[R(\mathbf{x}_i, \mathbf{x}_j)] = \begin{bmatrix} 1 & R(\mathbf{x}_1, \mathbf{x}_2) & \cdots & R(\mathbf{x}_1, \mathbf{x}_n) \\ R(\mathbf{x}_2, \mathbf{x}_1) & 1 & \cdots & R(\mathbf{x}_2, \mathbf{x}_n) \\ \vdots & \vdots & \ddots & \vdots \\ R(\mathbf{x}_n, \mathbf{x}_1) & R(\mathbf{x}_n, \mathbf{x}_2) & \cdots & 1 \end{bmatrix} \quad (36)$$

It is worth noting that not only the first-order derivative but also the second-order derivative for the MK shape function are need in the present plate theory. By taking the derivative of Eq. (29), these derivatives obtained as follows:

$$Z_{I,i}(\mathbf{x}) = \sum_{j=1}^m p_{j,i}(\mathbf{x})A_{jI} + \sum_{k=1}^n r_{k,i}(\mathbf{x})B_{kI} \quad (37)$$

$$Z_{I,ii}(\mathbf{x}) = \sum_{j=1}^m p_{j,ii}(\mathbf{x})A_{jI} + \sum_{k=1}^n r_{k,ii}(\mathbf{x})B_{kI} \quad (38)$$

On the other hand, the influence domain defined by either circle or sphere included the radius and a center located at the point of interest to determine the scattered nodes implementing the interpolation. This influence domain can be calculated by:

$$d_m = \alpha d_c \quad (39)$$

where d_c represents a characteristic length, α denotes a scaling factor. According to the numerical investigation in the work [22], we use a value of $\alpha = 2.1$ with the fine mesh of 21×21 for numerical analyses in this study. It should be pointed out that the MK shape function $Z_I(\mathbf{x}_j)$ satisfies the Kronecker delta at node \mathbf{x}_j

$$Z_I(\mathbf{x}_j) = \delta_{Ij} = \begin{cases} 1 & \text{for } I = j \\ 0 & \text{for } I \neq j \end{cases} \quad (40)$$

3.2. Discrete governing equations

The displacement field of the FGPP defined by Eq. (28) and can be expressed with respect to the nodal displacements as follows:

$$\tilde{\mathbf{u}}^h = \left[\tilde{u}_0^h \quad \tilde{v}_0^h \quad \tilde{w}_b^h \quad \tilde{w}_s^h \right]^T \quad (41)$$

and

$$\tilde{\mathbf{u}}_I = \left[\tilde{u}_{0,I} \quad \tilde{v}_{0,I} \quad \tilde{w}_{b,I} \quad \tilde{w}_{s,I} \right]^T \quad (42)$$

By substituting Eq. (28) into Eqs. (17) to (21), and the using some manipulations we obtain the strain expressions that given by:

$$\boldsymbol{\varepsilon}_1 = \sum_{I=1}^n \mathbf{B}_I^{b1} \tilde{\mathbf{u}}_I \quad (43)$$

$$\boldsymbol{\varepsilon}_2 = \sum_{I=1}^n \mathbf{B}_I^{b2} \tilde{\mathbf{u}}_I \quad (44)$$

$$\boldsymbol{\varepsilon}_3 = \sum_{I=1}^n \mathbf{B}_I^{b3} \tilde{\mathbf{u}}_I \quad (45)$$

$$\boldsymbol{\varepsilon}_5 = \sum_{I=1}^n \mathbf{B}_I^{b5} \tilde{\mathbf{u}}_I \quad (46)$$

$$\boldsymbol{\varepsilon}_4 = \sum_{I=1}^n \mathbf{B}_I^{b4} \tilde{\mathbf{u}}_I \quad (47)$$

in which \mathbf{B}_I^{b1} , \mathbf{B}_I^{b2} , \mathbf{B}_I^{b3} , \mathbf{B}_I^{b4} and \mathbf{B}_I^{b5} are defined by.

$$\mathbf{B}_I^{b1} = \begin{bmatrix} Z_{I,x} & 0 & 0 & 0 \\ 0 & Z_{I,y} & 0 & 0 \\ Z_{I,y} & Z_{I,x} & 0 & 0 \\ 0 & 0 & 0 & 0 \end{bmatrix} \quad (48)$$

$$\mathbf{B}_I^{b2} = \begin{bmatrix} 0 & 0 & -Z_{I,xx} & 0 \\ 0 & 0 & -Z_{I,yy} & 0 \\ 0 & 0 & -2Z_{I,xy} & 0 \\ 0 & 0 & 0 & 0 \end{bmatrix} \quad (49)$$

$$\mathbf{B}_I^{b3} = \begin{bmatrix} 0 & 0 & 0 & Z_{I,xx} \\ 0 & 0 & 0 & Z_{I,yy} \\ 0 & 0 & 0 & 2Z_{I,xy} \\ 0 & 0 & 0 & 0 \end{bmatrix} \quad (50)$$

$$\mathbf{B}_I^{b4} = \begin{bmatrix} 0 & 0 & 0 & 0 \\ 0 & 0 & 0 & 0 \\ 0 & 0 & 0 & 0 \\ 0 & 0 & 0 & Z_I \end{bmatrix} \quad (51)$$

$$\mathbf{B}_I^{b5} = \begin{bmatrix} 0 & 0 & 0 & Z_{I,x} \\ 0 & 0 & 0 & Z_{I,y} \end{bmatrix} \quad (52)$$

By utilizing the weak formulation [27], and using Eq. (22) and Eq. (26), the weak form of the FGPP laid on the elastic foundations for the static bending problem can be obtained as follows:

$$\begin{aligned} & \int_V \delta \boldsymbol{\varepsilon}^T \mathbf{D}^\varepsilon \boldsymbol{\varepsilon} dV + \int_V \delta \boldsymbol{\varepsilon}_5^T \mathbf{D}_5 \boldsymbol{\varepsilon}_5 dV + \int_\Theta \delta [w_b + w_{s,g}(z)] k_w [w_b + w_{s,g}(z)] d\Theta + \\ & \dots + \int_\Theta \nabla^T \delta [w_b + w_{s,g}(z)] k_s \nabla [w_b + w_{s,g}(z)] d\Theta = \int_\Theta \delta [w_b + w_{s,g}(z)] q_0 d\Theta \end{aligned} \quad (53)$$

in which

$$\boldsymbol{\varepsilon} = \begin{pmatrix} \boldsymbol{\varepsilon}_1 \\ \boldsymbol{\varepsilon}_2 \\ \boldsymbol{\varepsilon}_3 \\ \boldsymbol{\varepsilon}_4 \end{pmatrix} \quad (54)$$

$$\mathbf{D}^\varepsilon = \begin{bmatrix} \mathbf{T}^{\varepsilon 1} & \mathbf{T}^{\varepsilon 2} & \mathbf{T}^{\varepsilon 4} & \mathbf{T}^{\varepsilon 5} \\ \mathbf{T}^{\varepsilon 2} & \mathbf{T}^{\varepsilon 3} & \mathbf{T}^{\varepsilon 6} & \mathbf{T}^{\varepsilon 7} \\ \mathbf{T}^{\varepsilon 4} & \mathbf{T}^{\varepsilon 6} & \mathbf{T}^{\varepsilon 8} & \mathbf{T}^{\varepsilon 9} \\ \mathbf{T}^{\varepsilon 5} & \mathbf{T}^{\varepsilon 7} & \mathbf{T}^{\varepsilon 9} & \mathbf{T}^{\varepsilon 10} \end{bmatrix} \quad (55)$$

$$\mathbf{D}_5 = \int_{-h/2}^{h/2} \mathbf{D}^s(z) dz \quad (56)$$

where

$$\{T_{ij}^{\varepsilon 1}, T_{ij}^{\varepsilon 2}, T_{ij}^{\varepsilon 3}, T_{ij}^{\varepsilon 4}, T_{ij}^{\varepsilon 5}\} = \int_{-h/2}^{h/2} \{1, z, z^2, f(z), g'(z)\} \tilde{Q}_{ij}(z) dz \quad (57)$$

$$D_{ij}^s = \int_{-h/2}^{h/2} [f'(z) + g(z)]^2 \tilde{G}_{ij}(z) dz \quad (58)$$

$$\{T_{ij}^{\varepsilon 6}, T_{ij}^{\varepsilon 7}, T_{ij}^{\varepsilon 8}, T_{ij}^{\varepsilon 9}, T_{ij}^{\varepsilon 10}\} = \int_{-h/2}^{h/2} \{zf(z), zg'(z), f^2(z), f(z)g'(z), g'^2(z)\} \tilde{Q}_{ij}(z) dz \quad (59)$$

and $\nabla^T = [\partial/\partial x \quad \partial/\partial y]^T$ is the gradient operator, $\tilde{\mathbf{Q}}(z)$ and $\tilde{\mathbf{G}}(z)$ are matrices determining the constitutive material behaviors.

$$\tilde{\mathbf{Q}}(z) = \begin{bmatrix} Q_{11}(z) & Q_{12}(z) & 0 & Q_{13}(z) \\ Q_{12}(z) & Q_{22}(z) & 0 & Q_{23}(z) \\ 0 & 0 & Q_{44}(z) & 0 \\ Q_{13}(z) & Q_{23}(z) & 0 & Q_{33}(z) \end{bmatrix} \quad (60)$$

$$\tilde{\mathbf{G}}(z) = \begin{bmatrix} Q_{55}(z) & 0 \\ 0 & Q_{66}(z) \end{bmatrix} \quad (61)$$

In the same way, the weak form for free vibration problem of the FGPP rested on the elastic foundations can be expressed as follows:

$$\begin{aligned} & \int_V \delta \boldsymbol{\varepsilon}^T \mathbf{D}^\varepsilon \boldsymbol{\varepsilon} dV + \int_V \delta \boldsymbol{\varepsilon}_5^T \mathbf{D}_s \boldsymbol{\varepsilon}_5 dV + \int_\Theta \delta [w_b + w_s g(z)] k_w [w_b + w_s g(z)] d\Theta + \dots \\ & \dots + \int_\Theta \nabla^T \delta [w_b + w_s g(z)] k_s \nabla [w_b + w_s g(z)] d\Theta = \int_V \delta \mathbf{u}^T \mathbf{m} \ddot{\mathbf{u}} dV \end{aligned} \quad (62)$$

in which

$$\mathbf{m} = \begin{bmatrix} \mathfrak{V}_1 & \mathfrak{V}_2 & \mathfrak{V}_4 & \mathfrak{V}_5 \\ \mathfrak{V}_2 & \mathfrak{V}_3 & \mathfrak{V}_6 & \mathfrak{V}_7 \\ \mathfrak{V}_4 & \mathfrak{V}_6 & \mathfrak{V}_8 & \mathfrak{V}_9 \\ \mathfrak{V}_5 & \mathfrak{V}_7 & \mathfrak{V}_9 & \mathfrak{V}_{10} \end{bmatrix} \quad (63)$$

$$\{\mathfrak{V}_1, \mathfrak{V}_2, \mathfrak{V}_3, \mathfrak{V}_4, \mathfrak{V}_5\} = \int_{-h/2}^{h/2} \rho(z) \{1, z, z^2, f(z), g(z)\} dz \quad (64)$$

$$\{\mathfrak{V}_6, \mathfrak{V}_7, \mathfrak{V}_8, \mathfrak{V}_9, \mathfrak{V}_{10}\} = \int_{-h/2}^{h/2} \rho(z) \{zf(z), zg(z), f^2(z), f(z)g(z), g^2(z)\} dz \quad (65)$$

and $\mathbf{u}_1, \mathbf{u}_2, \mathbf{u}_3, \mathbf{u}_4$ can be obtained by substitution Eq. (28) in Eq. (10), they can be expressed as follows:

$$\mathbf{u} = \{ \mathbf{u}_1 \quad \mathbf{u}_2 \quad \mathbf{u}_3 \quad \mathbf{u}_4 \}^T \quad (66)$$

$$\mathbf{u}_1 = \sum_{I=1}^n \mathbf{N}_I^1 \tilde{\mathbf{u}}_I \quad (67)$$

$$\mathbf{u}_2 = \sum_{I=1}^n \mathbf{N}_I^2 \tilde{\mathbf{u}}_I \quad (68)$$

$$\mathbf{u}_3 = \sum_{I=1}^n \mathbf{N}_I^3 \tilde{\mathbf{u}}_I \quad (69)$$

$$\mathbf{u}_4 = \sum_{I=1}^n \mathbf{N}_I^4 \tilde{\mathbf{u}}_I \quad (70)$$

where

$$\mathbf{N}_I^1 = \begin{bmatrix} Z_I & 0 & 0 & 0 \\ 0 & Z_I & 0 & 0 \\ 0 & 0 & Z_I & 0 \end{bmatrix} \quad (71)$$

$$\mathbf{N}_I^2 = \begin{bmatrix} 0 & 0 & -Z_{I,x} & 0 \\ 0 & 0 & -Z_{I,y} & 0 \\ 0 & 0 & 0 & 0 \end{bmatrix} \quad (72)$$

$$\mathbf{N}_I^3 = \begin{bmatrix} 0 & 0 & 0 & Z_{I,x} \\ 0 & 0 & 0 & Z_{I,y} \\ 0 & 0 & 0 & 0 \end{bmatrix} \quad (73)$$

$$\mathbf{N}_I^4 = \begin{bmatrix} 0 & 0 & 0 & 0 \\ 0 & 0 & 0 & 0 \\ 0 & 0 & 0 & Z_I \end{bmatrix} \quad (74)$$

By substituting the displacement field defined by Eq. (42) and the strain tensor defined by Eqs. (43) to (47) into the weak forms derived by Eq. (53) and Eq. (62), we obtain the discretized equations for the static bending, free vibration problems of the FGPP laid on the elastic foundations as follows:

$$\mathbf{K}_\Delta \mathbf{u} = \mathbf{f} \quad (75)$$

$$(\mathbf{K}_\Delta - \Omega^2 \mathbf{M}_\Delta) \mathbf{u} = \mathbf{0} \quad (76)$$

where \mathbf{K} is the global stiffness matrix, it can be expressed by

$$\begin{aligned} \mathbf{K}_\Delta = & \int_V \left\{ \begin{matrix} \mathbf{B}_I^{b1} \\ \mathbf{B}_I^{b2} \\ \mathbf{B}_I^{b3} \\ \mathbf{B}_I^{b4} \end{matrix} \right\}^T \left[\begin{matrix} \mathbf{T}^{\varepsilon 1} & \mathbf{T}^{\varepsilon 2} & \mathbf{T}^{\varepsilon 4} & \mathbf{T}^{\varepsilon 5} \\ \mathbf{T}^{\varepsilon 2} & \mathbf{T}^{\varepsilon 3} & \mathbf{T}^{\varepsilon 6} & \mathbf{T}^{\varepsilon 7} \\ \mathbf{T}^{\varepsilon 4} & \mathbf{T}^{\varepsilon 6} & \mathbf{T}^{\varepsilon 8} & \mathbf{T}^{\varepsilon 9} \\ \mathbf{T}^{\varepsilon 5} & \mathbf{T}^{\varepsilon 7} & \mathbf{T}^{\varepsilon 9} & \mathbf{T}^{\varepsilon 10} \end{matrix} \right] \left\{ \begin{matrix} \mathbf{B}_I^{b1} \\ \mathbf{B}_I^{b2} \\ \mathbf{B}_I^{b3} \\ \mathbf{B}_I^{b4} \end{matrix} \right\} dV + \int_V (\mathbf{B}_I^{b5})^T \mathbf{D}_s \mathbf{B}_I^{b5} dV \\ & + \int_\Theta \mathbf{N}_I^T k_w \mathbf{N}_I d\Theta + \dots + \int_\Theta k_s \left[(\mathbf{B}_I^{g1})^T \mathbf{B}_I^{g1} + (\mathbf{B}_I^{g2})^T \mathbf{B}_I^{g2} \right] d\Theta \end{aligned} \quad (77)$$

and \mathbf{f} denotes the externally applied loads given by the vector as follows:

$$\mathbf{f} = \int_\Theta q_0 \mathbf{N}_I d\Theta \quad (78)$$

with

$$\mathbf{N}_I = \begin{bmatrix} 0 & 0 & Z_I & 0 \end{bmatrix}^T \quad (79)$$

The global mass matrix \mathbf{M}_Δ defined by:

$$\mathbf{M}_\Delta = \int_V \begin{Bmatrix} \mathbf{N}_I^1 \\ \mathbf{N}_I^2 \\ \mathbf{N}_I^3 \\ \mathbf{N}_I^4 \end{Bmatrix}^T \begin{bmatrix} \mathfrak{J}_1 & \mathfrak{J}_2 & \mathfrak{J}_4 & \mathfrak{J}_5 \\ \mathfrak{J}_2 & \mathfrak{J}_3 & \mathfrak{J}_6 & \mathfrak{J}_7 \\ \mathfrak{J}_4 & \mathfrak{J}_6 & \mathfrak{J}_8 & \mathfrak{J}_9 \\ \mathfrak{J}_5 & \mathfrak{J}_7 & \mathfrak{J}_9 & \mathfrak{J}_{10} \end{bmatrix} \begin{Bmatrix} \mathbf{N}_I^1 \\ \mathbf{N}_I^2 \\ \mathbf{N}_I^3 \\ \mathbf{N}_I^4 \end{Bmatrix} dV \quad (80)$$

where

$$\mathbf{B}_I^{g1} = \begin{bmatrix} 0 & 0 & Z_{I,x} & 0 \\ 0 & 0 & Z_{I,y} & 0 \end{bmatrix} \quad (81)$$

$$\mathbf{B}_I^{g2} = \begin{bmatrix} 0 & 0 & 0 & Z_{I,x} \\ 0 & 0 & 0 & Z_{I,y} \end{bmatrix} \quad (82)$$

It is worth mentioning that matrices \mathbf{B}_I^{b2} defined by Eq. (48) and \mathbf{B}_I^{b3} Eq. (50) comprising the second-order derivatives of the MK shape function; hence the displacement field of the plate should be C^1 -continuity. Hence, a second-order polynomial basis is used for Eq. (32) as follows:

$$p^T(\mathbf{x}) = \{ 1 \quad x \quad y \quad x^2 \quad xy \quad y^2 \} \quad (83)$$

Moreover, the quadratic polynomial basic function ($m = 6$) and the background mesh with (4×4) Gauss points are used for building the MK shape function.

4. Numerical results

In this section, we present our solutions of the static bending, natural frequencies of the rectangular FGPP laid on the elastic foundations chosen as Winkler or Pasternak foundation model. The present results are computed by using the novel refined quasi-3D sinusoidal shear deformation theory with only four variables combined with the moving Kriging interpolation-based meshfree method. To illustrate the accuracy of the proposed approach, a ceramic-metal functionally graded plate is considered. The Young's modulus and density of alumina are $E_c = 380$ GPa and $\rho_c = 3800$ kg/m³, while those of aluminum are $E_m = 70$ GPa and $\rho_m = 2702$ kg/m³, respectively. The Poisson's ratios for both aluminum and alumina are taken $\nu = 0.3$. For convenience, the normalized parameters are utilized in this section as follows [20]:

$$K_w^m = \frac{k_w a^4}{D_m} \quad (84)$$

$$K_s^m = \frac{k_s a^2}{D_m} \quad (85)$$

$$K_s^m = \frac{k_s a^2}{D_m} \quad (86)$$

$$D_m = \frac{E_m h^3}{12(1-\nu^2)} \quad (87)$$

$$w_c^m = \frac{10E_c h^3}{a^4 q_0} w \left(\frac{a}{2}, \frac{b}{2}, 0 \right) \quad (88)$$

$$\Omega_m = \Omega \frac{a^2}{h} \sqrt{\frac{\rho_m}{E_m}} \quad (89)$$

4.1. Static bending analysis of the FGPP

In order to verify the accuracy of proposed approach, we calculated the central deflection w_c^m of the full-simply supported square FGPP with the gradient index $\chi = 1$ subjected to a sinusoidal load with the various thickness-to-length ratios h/a and the elastic foundation parameters (K_w^m, K_s^m). Three types of porous laws are considered (POR-1), (POR-2), and (POR-3) in this verification. The obtained results are compared with quasi-3D solutions given by Kaddari et al. [20] as shown in Table 1. These results are predicted by the shear and normal deformation theories that take into account the stretching effect. From table results, it can be observed that our results are in good agreement for all values of the thickness-to-length ratios h/a , elastic foundation parameters and the porosity volume fractions. It is notable that Kaddari et al. [20] used the quasi-3D plate model based on five unknown displacements with the indeterminate integral variables and employed the Navier technique for the governing equations getting the closed-form solutions. It can be seen that the displacements w_c^m decrease with regarding to the elastic foundations, moreover the central deflections w_c^m of the FGPP rested on the Winkler's foundation are greater than those of the FGPP laid on the Pasternak's foundation. Increasing the thickness-to-length ratios h/a leads to increase the displacements of FGPP. The central displacements of the FGPP with the even porosity distribution are greater than those of the FGPP with the uneven porosity distributions at the certain thickness-to-length ratios under the sinusoidal load.

Table 1. Comparisons of the normalized center deflection w_c^m of square FGPP subjected to sinusoidal load resting on Winkler–Pasternak foundations

$\left(\frac{K_w^m}{K_s^m}\right)$	$\frac{h}{a}$	Methods	POR-1		POR-2		POR-3	
			$p = 0.2$	$p = 0.5$	$p = 0.2$	$p = 0.5$	$p = 0.2$	$p = 0.50$
$\left(\frac{0}{0}\right)$	0.05	Ref. [20]	0.7576	2.2899	0.5974	0.6903	0.5951	0.6707
		Present	0.7850	2.3652	0.6184	0.7127	0.6160	0.6929
		Error [%]	3.62	3.29	3.52	3.25	3.51	3.31
	0.10	Ref. [20]	0.7797	2.3254	0.6180	0.7173	0.6155	0.6963
		Present	0.7996	2.3887	0.6314	0.7283	0.6289	0.7080
		Error [%]	2.55	2.72	2.17	1.54	2.18	1.67
0.20	Ref. [20]	0.8675	2.4657	0.6995	0.8243	0.6963	0.7976	
	Present	0.8623	2.4896	0.6878	0.7968	0.6850	0.7740	
	Error [%]	-0.59	0.97	-1.67	-3.33	-1.62	-2.96	
$\left(\frac{10^2}{0}\right)$	0.05	Ref. [20]	0.6719	1.6523	0.5428	0.6184	0.5409	0.6027
		Present	0.6933	1.6912	0.5601	0.6146	0.5581	0.6205
		Error [%]	3.19	2.36	3.18	-0.62	3.18	2.95
	0.10	Ref. [20]	0.6897	1.6721	0.5601	0.6404	0.5580	0.6236
		Present	0.7047	1.7032	0.5707	0.6487	0.5687	0.6325
		Error [%]	2.17	1.86	1.90	1.30	1.92	1.43
0.20	Ref. [20]	0.7585	1.7473	0.6269	0.7253	0.6244	0.7046	
	Present	0.7531	1.7545	0.6165	0.7027	0.6143	0.6849	
	Error [%]	-0.71	0.41	-1.66	-3.12	-1.62	-2.80	
$\left(\frac{10^2}{10^2}\right)$	0.05	Ref. [20]	0.2078	0.2544	0.1936	0.2024	0.1934	0.2007
		Present	0.2091	0.2542	0.1951	0.2029	0.1948	0.2019
		Error [%]	0.61	-0.06	0.76	0.25	0.74	0.61
	0.10	Ref. [20]	0.2103	0.2554	0.1965	0.2054	0.1962	0.2037
		Present	0.2101	0.2545	0.1964	0.2049	0.1961	0.2032
		Error [%]	-0.09	-0.34	-0.06	-0.27	-0.03	-0.24
0.20	Ref. [20]	0.2177	0.2584	0.2055	0.2149	0.2052	0.2130	
	Present	0.2145	0.2559	0.2018	0.2100	0.2016	0.2086	
	Error [%]	-1.47	-0.98	-1.80	-2.28	-1.78	-2.06	

After validation of the formulations of present RQSSDT for static bending of the square FGPP embedded in the elastic foundation through comparison studies with the available quasi-3D results, the effects of the gradient index and aspect ratios on the deflection of the plate subjected to the sinusoidal load is examined. For this purpose, three types of pore distribution (POR-1), (POR-2) and (POR-3) are utilized. Fig. 2 shows the variations of the normalized center deflection w_c^m of the FGPP with porosity factor $\vartheta = 0.2$ versus the gradient index χ at a constant value of the thickness-to-length ratio ($h/a = 0.1$).

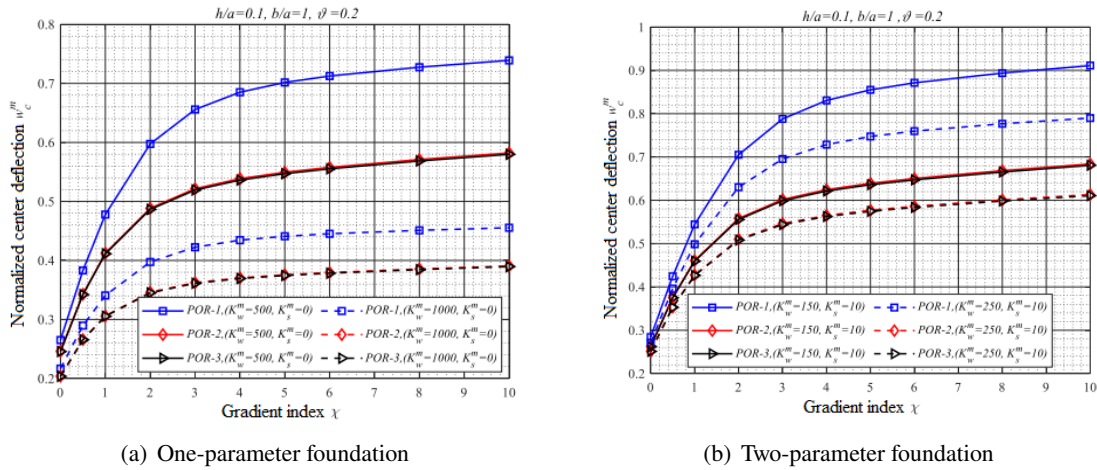


Figure 2. Variations of the normalized center deflection w_c^m of the FGPP (with porosity factor $\vartheta = 0.2$) versus the gradient index χ for differences of stiffness foundation parameters

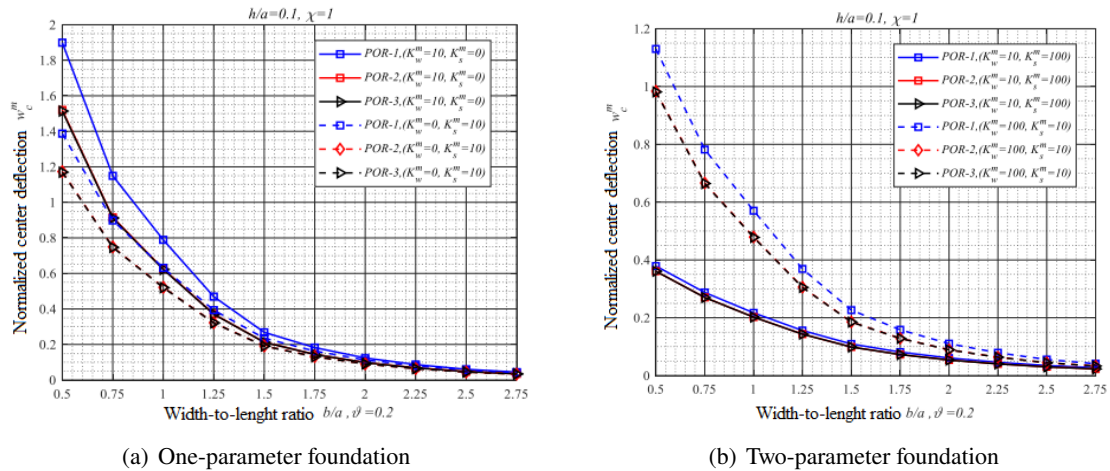


Figure 3. Variations of the normalized center deflection w_c^m of the FGPP (with porosity factor $\vartheta = 0.2$) versus the aspect ratio b/a

It is clear that the gradient index has no stiffness-softening effect on the static bending of the FGPP resting on the elastic foundations. Moreover, increasing the gradient index leads to the deflections of the FGPP with the even porous (POR-1) greater than those with the uneven porous (POR-2, POR-3). Furthermore, the shear stiffness foundations K_s^m are more effects than the spring stiffness foundations K_w^m for the deflections of the FGPP. Fig. 3 shows the variations of the normalized center deflection of the FGPP versus the aspect ratio b/a at the constant value of the gradient index $\chi = 1$. It can be seen

that the deflection of the FGPP rested on the elastic foundations converges to the certain values when increasing the plate aspect ratios, since the behavior of the plate FGPP similar to the one-way plate, wherein only its short side is effective.

4.2. Free vibration analysis of the FGPP

To validate the accuracy of the proposed theory with EMKI based meshfree method for the free vibration analyses of the FGPP resting on the elastic foundations, we calculated the first natural frequencies Ω_m of the plate by using the proposed approach.

Table 2. Comparisons of the first non-dimensional natural frequency Ω_m of the square FGPP resting on Winkler–Pasternak foundations

$\left(\frac{K_w^m}{K_s^m}\right)$	$\frac{h}{a}$	Methods	POR-1		POR-2		POR-3	
			$p = 0.2$	$p = 0.5$	$p = 0.2$	$p = 0.5$	$p = 0.2$	$p = 0.50$
$\left(\frac{0}{0}\right)$	0.05	Ref. [20]	8.3700	5.7380	9.0510	9.1160	9.0530	9.1050
		Ref. [19]	8.3700	5.7380	9.0520	9.1170	9.0500	9.1060
		Present	8.1629	5.9707	8.6674	8.8449	8.6619	8.8140
		Error [%]	-2.47	4.05	-4.25	-2.98	-4.29	-3.21
	0.10	Ref. [20]	8.2030	5.6590	8.8420	8.8950	8.8590	8.8870
		Ref. [19]	8.2030	5.6590	8.8450	8.8960	8.8430	8.8890
		Present	8.0150	5.8887	8.4973	8.6635	8.4920	8.6347
		Error [%]	-2.29	4.06	-3.93	-2.61	-3.97	-2.86
	0.15	Ref. [20]	-	-	-	-	-	-
		Ref. [19]	7.9500	5.5350	8.5360	8.5690	8.5350	8.5650
		Present	7.7852	5.7600	8.2333	8.3812	8.2287	8.3557
		Error [%]	-2.07	4.06	-3.55	-2.19	-3.59	-2.44
0.20	Ref. [20]	7.6410	5.3780	8.1530	8.1770	8.2250	8.1770	
	Ref. [19]	7.6410	5.3780	8.1640	8.1780	8.1630	8.1780	
	Present	7.4975	5.5954	7.9040	8.0280	7.9001	8.0070	
	Error [%]	-1.88	4.04	-3.18	-1.83	-3.22	-2.09	
$\left(\frac{10^2}{0}\right)$	0.05	Ref. [20]	8.9170	6.9330	9.5030	9.6530	9.5040	9.6240
		Ref. [19]	8.9170	6.9330	9.5050	9.6550	9.5010	9.6260
		Present	8.7231	7.1267	9.1394	9.3976	9.1318	9.3500
		Error [%]	-2.17	2.79	-3.85	-2.67	-3.89	-2.87
	0.10	Ref. [20]	8.7500	6.8480	9.2960	9.4340	9.3120	9.4080
		Ref. [19]	8.7530	6.8500	9.3010	9.4380	9.2980	9.4120
		Present	8.5741	7.0386	8.9688	9.2157	8.9615	9.1701
		Error [%]	-2.04	2.75	-3.57	-2.36	-3.62	-2.57
	0.15	Ref. [20]	-	-	-	-	-	-
		Ref. [19]	8.5050	6.7210	8.9990	9.1180	8.9950	9.0960
		Present	8.3437	6.9012	8.7052	8.9339	8.6984	8.8916
		Error [%]	-1.90	2.68	-3.27	-2.02	-3.30	-2.25
0.20	Ref. [20]	8.1960	6.5530	8.6170	8.7290	8.7090	8.7110	
	Ref. [19]	8.2030	6.5590	8.6360	8.7380	8.6320	8.7190	
	Present	8.0571	6.7272	8.3779	8.5834	8.3718	8.5454	
	Error [%]	-1.78	2.56	-2.99	-1.77	-3.01	-1.99	
$\left(\frac{10^2}{10^2}\right)$	0.05	Ref. [20]	16.3130	18.6210	16.0020	17.0890	15.9750	16.8710
		Ref. [19]	16.3200	18.6250	16.0110	17.0980	15.9820	16.8000
		Present	16.2104	18.6948	15.7937	16.9516	15.7621	16.7210
		Error [%]	-0.67	0.37	-1.36	-0.86	-1.38	-0.47
	0.1	Ref. [20]	16.1180	18.4460	15.7770	16.8500	15.7580	16.6350
		Ref. [19]	16.1480	18.4640	15.8120	16.8830	15.7830	16.6680
		Present	16.0146	18.5083	15.5864	16.7247	15.5552	16.4981
		Error [%]	-0.83	0.24	-1.43	-0.94	-1.44	-1.02
	0.15	Ref. [20]	-	-	-	-	-	-
		Ref. [19]	15.8950	18.2120	15.5250	16.5750	15.5000	16.3650
		Present	15.7199	18.2197	15.2745	16.3833	15.2442	16.1625
		Error [%]	-1.10	0.04	-1.61	-1.16	-1.65	-1.24
0.20	Ref. [20]	15.4770	17.7310	15.0730	16.1000	15.0800	15.8960	
	Ref. [19]	15.5950	17.8720	15.1920	16.2210	15.1640	16.0160	
	Present	15.3686	17.8616	14.9036	15.9778	14.8742	15.7640	
	Error [%]	-1.45	-0.06	-1.90	-1.50	-1.91	-1.57	

Table 2 shows the comparison of the first non-dimensional natural frequencies for various values of the ratios h/a and non-dimensional stiffness foundations (K_w^m, K_s^m). It can be concluded that there is good agreement between the present results and those generated by the reference quasi-3D methods given by Kaddari et al. [20] and Shahsavari et al. [19]. It is worth noting that Shahsavari et al. [19] utilized the quasi-3D hyperbolic shear deformation plate theory used five unknown variables for modeling the displacement fields, and obtained the analytical solutions by using the Galerkin's method for solving the governing equations. It is worth noting that the first natural frequencies Ω_m of the FGPP increase with regarding to the elastic foundations. Moreover, the first natural frequencies Ω_m of the FGPP rested on the Winker's foundation model are smaller than those of the FGPP laid on the Pasternak's foundation model. Increasing the thickness-to-length ratio h/a leads to decrease the first natural frequencies of FGPP. The fundamental natural frequencies of the FGPP with the even porosity distribution smaller than those with the uneven porosity distributions at certain thickness-to-length ratios. The effects of the gradient index χ on the natural frequency of the square FGPP rested on the elastic foundations are shown in Fig. 4. For the elastic foundations with spring stiffness parameters, it is worth noting that the gradient index has the stiffness-softening effect on its natural frequencies, moreover, the FGPP with even porosity distribution (POR-1) features the natural frequency smaller than those of the FGPP with uneven porosity distribution (POR-2, POR-3).

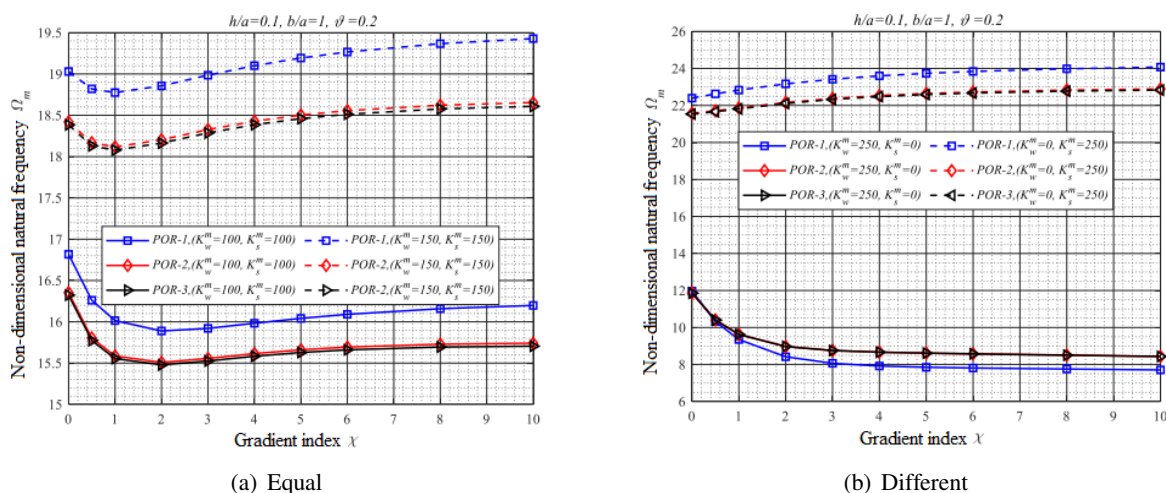


Figure 4. Variations of the first non-dimensional natural frequency Ω_m of the FGPP (with porosity factor $\vartheta = 0.2$) versus the gradient index χ for differences of spring stiffness foundation parameters

Meanwhile, in the case $\chi \geq 3$ the gradient index has the stiffness-softening effect on the natural frequencies of the FGPP laid on the elastic foundations with shear stiffness parameters, furthermore, the FGPP with even porosity distribution (POR-1) generates the natural frequency greater than those of the FGPP with uneven porosity distribution (POR-2, POR-3).

Fig. 5 shows the variations of the non-dimensional natural frequencies of the FGPP with respect to the aspect ratio b/a at the constant value of the gradient index $\chi = 1$. It can be seen that increasing the aspect ratios lead to increase the natural frequencies of the FGPP with and without the elastic foundations. Moreover, the FGPP with even porosity distribution (POR-1) generates the natural frequency smaller than those of the FGPP with uneven porosity distribution (POR-2, POR-3) at high values of the aspect ratios. It is noteworthy that in the elastic foundations possessed values of the spring layer

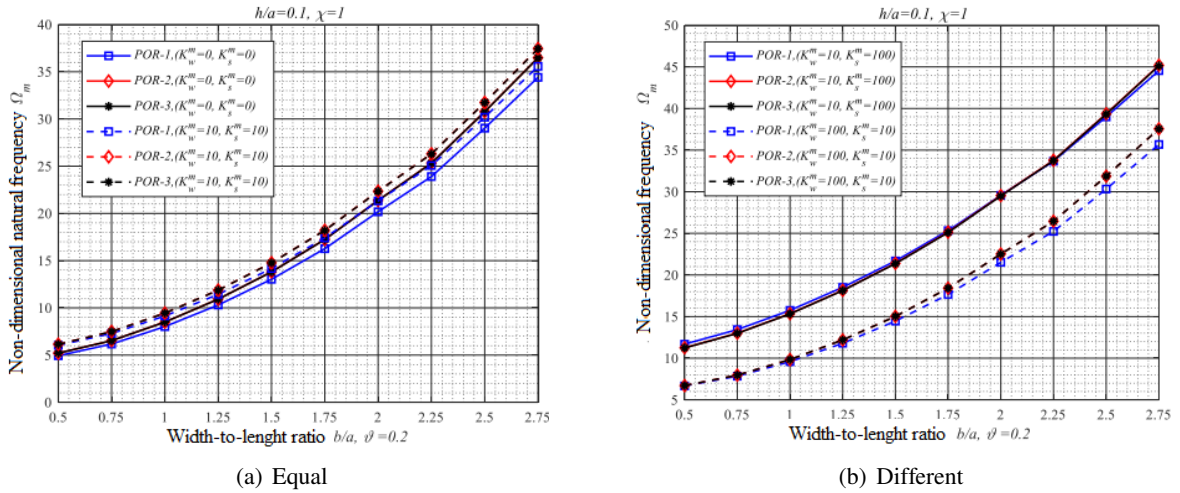


Figure 5. Variations of the first non-dimensional natural frequency Ω_m of the FGPP (with porosity factor $\theta = 0.2$) versus the aspect ratio b/a in the case of the values foundation parameters

are equal or larger than those of the shear layer, the maximum natural frequencies are belonging to the FGPP containing the uneven porosities (POR-2, POR-3).

5. Conclusions

In this article, a refined quasi-3D sinusoidal shear deformation theory combined with the moving Kriging interpolation-based meshfree method for the static bending and free vibration analysis of the FGPP laid on the elastic Pasternak foundations is proposed. Three porosity distributions for the FGPP are considered here, including the even, uneven and logarithmic-uneven distribution patterns. The accuracy of the present method is verified by comparing the obtained results with the available solutions. A comprehensive parametric study is carried out to assess the effects of volume fraction index, porosity fraction index, stiffness of foundation parameters, mode numbers, and geometry on the natural frequencies of imperfect FGPP. The following major points can be drawn from the present study as follows:

- The results generated by the presented refined quasi-3D sinusoidal shear deformation theory plate model show good agreement with the quasi-3D results in the available literature.
- The presented refined quasi-3D sinusoidal theory is efficient, and easy to implement since the number of unknown variables involved in the present theory is only four, compared with other quasi-3D theories containing five unknown variables.
- The FGPP with the even porosity distribution generates the displacements greater than those of the FGPP with the uneven porosity distributions at the certain thickness-to-length ratios. The deflections of the FGPP with the even porous (POR-1) greater than those of the FGPP with the uneven porous (POR-2, POR-3) when increasing the gradient index.
- Natural frequencies of the FGPP with the even porosity distribution are smaller than those of the FGPP with the uneven porosity distributions at the certain thickness-to-length ratios in the case of the FGPP laid on the Winker's foundation or without elastic foundations.
- The FGPP with even porosity distribution (POR-1) generates the natural frequency smaller than those of the FGPP with uneven porosity distribution (POR-2, POR-3) at high values of the aspect

ratios. For the Pasternak elastic foundation characterized by the spring layer are equal or larger than the shear layer, the maximum natural frequencies are belonging to the FGPP with the uneven porosities (POR-2, POR-3).

Acknowledgements

This research is funded by the Vietnam National Foundation for Science and Technology Development (NAFOSTED) under grant number 107.01-2018.319. The authors gratefully acknowledge for this financial support.

References

- [1] Wang, Y. Q., Zu, J. W. (2017). [Vibration behaviors of functionally graded rectangular plates with porosities and moving in thermal environment](#). *Aerospace Science and Technology*, 69:550–562.
- [2] Phuong, N. T. B., Tu, T. M., Phuong, H. T., Van Long, N. (2019). [Bending analysis of functionally graded beam with porosities resting on elastic foundation based on neutral surface position](#). *Journal of Science and Technology in Civil Engineering (STCE)-NUCE*, 13(1):33–45.
- [3] WinNler, E. (1867). *Die Lehre von der Elastizität und Festigkeit (The Theory of Elasticity and Stiffness)*. Prague: H. Dominus.
- [4] Pasternak, P. L. (1954). *New calculation method for flexible substructures on a two-parameter elastic foundation*. Stroyizdat, Moskva.
- [5] Kerr, A. D. (1964). [Elastic and viscoelastic foundation models](#). *Journal of Applied Mechanics*, 31(3): 491–498.
- [6] Kirchhoff, G. (1850). *Über das Gleichgewicht und die Bewegung einer elastischen Scheibe*, volume 40. *Journal für die Reine und Angewandte Mathematik*, 51–88.
- [7] Mindlin, R. D. (1951). [Influence of rotatory inertia and shear on flexural motions of isotropic, elastic plates](#). *Journal of Applied Mechanics*, 18:31–38.
- [8] Reissner, E. (1945). [The effect of transverse shear deformation on the bending of elastic plates](#). *Journal of Applied Mechanics*, 12(2):69–77.
- [9] Reddy, J. N. (1984). [A simple higher-order theory for laminated composite plates](#). *Journal of Applied Mechanics*, 51(4):745–752.
- [10] Shimpi, R. P. (2002). [Refined plate theory and its variants](#). *AIAA Journal*, 40(1):137–146.
- [11] Carrera, E., Brischetto, S., Cinefra, M., Soave, M. (2011). [Effects of thickness stretching in functionally graded plates and shells](#). *Composites Part B: Engineering*, 42(2):123–133.
- [12] Carrera, E., Miglioretti, F., Petrolo, M. (2011). [Accuracy of refined finite elements for laminated plate analysis](#). *Composite Structures*, 93(5):1311–1327.
- [13] Talha, M., Singh, B. N. (2010). [Static response and free vibration analysis of FGM plates using higher order shear deformation theory](#). *Applied Mathematical Modelling*, 34(12):3991–4011.
- [14] Ganapathi, M., Makhecha, D. P. (2001). [Free vibration analysis of multi-layered composite laminates based on an accurate higher-order theory](#). *Composites Part B: Engineering*, 32(6):535–543.
- [15] Chen, C.-S., Hsu, C.-Y., Tzou, G. J. (2009). [Vibration and stability of functionally graded plates based on a higher-order deformation theory](#). *Journal of Reinforced Plastics and Composites*, 28(10):1215–1234.
- [16] Reddy, J. N. (2011). [A general nonlinear third-order theory of functionally graded plates](#). *International Journal of Aerospace and Lightweight Structures (IJALS)*, 1(1).
- [17] Long, N. V., Quoc, T. H., Tu, T. M. (2016). [Bending and free vibration analysis of functionally graded plates using new eight-unknown shear deformation theory by finite-element method](#). *International Journal of Advanced Structural Engineering*, 8(4):391–399.
- [18] Tu, T. M., Quoc, T. H., Long, N. V. (2017). [Bending analysis of functionally graded plates using new eight-unknown higher order shear deformation theory](#). *Structural Engineering and Mechanics*, 62(3): 311–324.

- [19] Shahsavari, D., Shahsavari, M., Li, L., Karami, B. (2018). [A novel quasi-3D hyperbolic theory for free vibration of FG plates with porosities resting on Winkler/Pasternak/Kerr foundation](#). *Aerospace Science and Technology*, 72:134–149.
- [20] Kaddari, M., Kaci, A., Bousahla, A. A., Tounsi, A., Bourada, F., Tounsi, A., Bedia, E. A., Al-Osta, M. A. (2020). [A study on the structural behaviour of functionally graded porous plates on elastic foundation using a new quasi-3D model: bending and free vibration analysis](#). *Computers and Concrete*, 25(1):37–57.
- [21] Zenkour, A. M. (2013). [A simple four-unknown refined theory for bending analysis of functionally graded plates](#). *Applied Mathematical Modelling*, 37(20-21):9041–9051.
- [22] Vu, T.-V., Curiel-Sosa, J. L., Bui, T. Q. (2019). [A refined sin hyperbolic shear deformation theory for sandwich FG plates by enhanced meshfree with new correlation function](#). *International Journal of Mechanics and Materials in Design*, 15(3):647–669.
- [23] Wattanasakulpong, N., Ungbhakorn, V. (2014). [Linear and nonlinear vibration analysis of elastically restrained ends FGM beams with porosities](#). *Aerospace Science and Technology*, 32(1):111–120.
- [24] Arya, H., Shimpi, R. P., Naik, N. K. (2002). [A zigzag model for laminated composite beams](#). *Composite Structures*, 56(1):21–24.
- [25] Shames, I. (2018). *Energy and finite element methods in structural mechanics*. CRC Press, New York.
- [26] Gu, L. (2003). [Moving kriging interpolation and element-free Galerkin method](#). *International Journal for Numerical Methods in Engineering*, 56(1):1–11.
- [27] Reddy, J. N. (2005). *Introduction to the finite element method*. McGraw-Hill New York.